A role for the Perlman syndrome exonuclease Dis3l2 in the Lin28-let-7 pathway

Published in final edited form as:
Nature. 2013 May 9; 497(7448): 244–248. doi:10.1038/nature12119.

A role for the Perlman syndrome exonuclease Dis3l2 in the Lin28-let-7 pathway

Hao-Ming Chang[1], **Robinson Triboulet**[1], **James E. Thornton**[1], and **Richard I. Gregory**[1,2]

[1]Stem Cell Program, Boston Children's Hospital, MA 02115. Department of Biological Chemistry and Molecular Pharmacology, Harvard Medical School, Boston, MA 02115, Harvard Stem Cell Institute, Boston, MA 02115

Abstract

The pluripotency factor Lin28 blocks the expression of let-7 microRNAs (miRNAs) in undifferentiated cells during development and functions as an oncogene in a subset of cancers[1]. Lin28 binds to let-7 precursor RNAs and recruits 3′ terminal uridylyl transferases (TUTases) to selectively inhibit let-7 biogenesis[2–4]. Uridylated pre-let-7 is refractory to processing by Dicer and is rapidly degraded by an unknown ribonuclease[5]. Here we identify Dis3l2 as the 3′-5′ exonuclease responsible for the decay of uridylated pre-let-7. Biochemical reconstitution assays reveal that 3′ oligouridylation stimulates Dis3l2 activity in vitro, and knockdown of Dis3l2 in mouse embryonic stem cells leads to the stabilization of pre-let-7. Our study establishes 3′ oligouridylation as an RNA decay signal for Dis3l2 and identifies the first physiological RNA substrate of this novel exonuclease that is mutated in the Perlman syndrome of fetal overgrowth and predisposition to Wilms' tumor[6].

Keywords

Dis3l2; exonuclease; uridylation; Lin-28; Lin28; let-7; microRNA (miRNA); TUTase; Embryonic Stem Cells

Posttranscriptional gene regulation by miRNAs impacts many developmental and physiological processes. Functioning by base-pairing with target messenger RNAs of complementary sequence these ~22 nucleotides RNAs recruit the miRNA-induced silencing complex for translational repression and mRNA decay. Of particular relevance is the ancient let-7 family of miRNAs that are essential for normal development of *C. elegans*. Loss of their tumor suppressor function impacts various human cancers[7]. Let-7 expression is dynamically regulated during development by the paralogous RNA-binding proteins Lin28A and Lin28B[5,8–10]. Lin28 was identified as a regulator of developmental timing in worms, and more recently has been linked with controlling developmental timing and growth of mammals as well as maintaining glucose homeostasis[1,11–13]. Lin28 is a pluripotency factor in stem cells where its expression helps maintain an undifferentiated and proliferative state by blocking let-7 expression[14,15]. The Lin28-let-7 pathway is normally silenced in adult somatic cells yet expression of Lin28A or Lin28B is associated with a wide variety of

[2]Corresponding author: Richard I. Gregory, Phone: (617) 919-2273, Fax: (617) 730-0748, rgregory@enders.tch.harvard.edu.

AUTHOR CONTRIBUTIONS

H.C. designed and performed most of the experiments in Figures 1 and 2 and all of the experiments in Figure 4. H.C. R.T. and J.E.T designed and performed experiments in Figures 1–4 as well as the Supplementary Figures. R.I.G., and H.C., wrote the paper with input from R.T. and J.E.T. The authors 11 declare no competing financial interests.

human cancers[16,17]. Inhibition of this oncogenic pathway blocks the tumorigenicity of cancer cells[16].

Recent work has provided insight into the mechanisms underlying the Lin28-mediated selective regulation of let-7[18]. Lin28A functions in the cell cytoplasm where it recruits 3′ terminal uridylyl transferases (TUTase), Zcchc11 (TUT4) and Zcchc6 (TUT7), that adds an oligouridine tail to pre-let-7 to inhibit Dicer processing and is thought to serve as a signal for the rapid decay of the uridylated RNA by an unknown nuclease[2–5,16]. We sought to identify the downstream nuclease(s) and utilized a biochemical approach to isolate factors that specifically associate with uridylated pre-let-7 (Figure 1a, Supplementary Figure S1, and Supplementary Table 1). This analysis identified that Lin28A and Zcchc11 were associated with both RNAs whereas Dis3l2 [DIS3 mitotic control homolog (*S. cerevisiae*)-like 2], a 3′-5′ exonuclease, was specifically detected in the pre-let-7+14U purification (Figure 1b)[6]. These mass spectrometry data were confirmed by Western blot (Figure 1c). Co-immunoprecipitation (co-IP) assays using a mouse ESC line expressing Dox-inducible Flag-Lin28 transgene revealed that Zcchc11, Zcchc6, as well as Dis3l2 are detectable by Western blot in the Flag-Lin28A affinity eluate (Figure 1d). Additional co-IPs with Flag-TRBP, a cytoplasmic miRNA-binding protein, and Flag-Trim71, a cytoplasmic RNA binding protein highly expressed in ESCs, confirmed the specificity of the Dis3l2 association with Lin28 (Figure 1e)[15,19]. To address whether this association is mediated through RNA we performed additional co-IPs using either wild-type Lin28 or a mutant Lin28 (W46A) protein that exhibits compromised RNA binding activity towards pre-let-7[18]. We found less Dis3l2 associated with mutant Lin28, and that this association is strongly reduced upon RNase A treatment (Figure 1f). Overall these results indicate that Lin28A associates with Dis3l2 in a RNA-dependent manner and implicate Dis3l2 as a possible nuclease in the Lin28-let-7 pathway.

We next cloned and sequenced Dis3l2 cDNA from ESCs. Dis3l2.2 was confirmed as the major transcript variant expressed in V6.5 ESC that encodes a 870 amino acid protein (Figure 1b and Supplementary Figure 2). Since pre-let-7 degradation occurs in the cell cytoplasm we next examined the subcellular localization of Dis3I2 in ESCs (Supplementary Figure 3). Dis3l2 was found to primarily localize to the cytoplasm of V6.5 ESC, which is consistent with other cell types[6].

We carried out RNA degradation assays using affinity-purified Flag-Dis3l2. Dis3l2 was found to preferentially degrade pre-let-7+14U over non-uridylated pre-let-7 or an unrelated pre-miR-21 (Figure 2a). To rule out the possibility that this observed activity was due to a co-purifying nuclease in the Flag-Dis3l2 IP we generated a mutant Dis3l2-expressing construct by replacing a conserved residue in the catalytic domain (D389N) (Figure 1b). Mutation of the equivalent Aspartic Acid in yeast DIS3 (D551N) abolishes exonuclease activity without interfering with RNA binding[20]. Indeed Dis3l2 displayed no activity whereas affinity-purified Dis3l2 displayed preferential activity towards pre-let--7+14U (Figures 2b–c).

Next, to determine whether Dis3l2 is sufficient for the selective degradation of uridylated pre-let-7 we generated recombinant Dis3l2 protein in *E. coli* (Figure 2d). Although the activity of recombinant Dis3l2 (rDis3l2) was lower than that of the affinity-purified Flag-Dis3l2 complexes we observed a similar preference for pre-let-7+14U compared with the non-uridylated pre-let-7 using the 5 recombinant Dis3l2 protein (Figures 2e–f). To rule out the possibility that this observed activity was due to a bacterial nuclease that might co-purify with His-Dis3l2 we generated a mutant (D389N) rDis3l2 and confirmed that this catalytic mutant displayed no ribonuclease activity in these assays (Supplementary Figure 4a). Considering that uridylated pre-let-7a-1 was previously found associated with isolated Flag-

Lin28A complexes together with our co-IP data, we next explored whether Lin28A protein influenced Dis3l2 activity in vitro[5]. This analysis revealed that Lin28A had no effect on Dis3l2 activity (Supplementary Figure 5). Next, to more quantitatively measure the substrate preference of Dis3l2 for uridylated pre-let-7 we performed time course experiments with rDis3l2. This revealed a strong preference for the degradation of uridylated pre-let-7 compared to non-uridylated pre-let-7, with >10-fold difference in the relative RNA stability in these assays (Figures 2g–h). Altogether these results reveal that purified recombinant Dis3l2 preferentially degrades uridylated pre-let-7 in vitro and the oligoU-tail serves as a decay signal for this ribonuclease.

To further explore the functional relationship between Lin28, TUTase, and Dis3l2-mediated RNA degradation we next performed in vitro reconstitution assays. Previously we showed that Lin28 enhances the uridylation activity of Zcchc11 towards pre-let-7. In these assays TUTase activity was measured by the incorporation of radiolabeled UTP[3,4,16]. However due to limiting UTP concentration the oligo-U tails added in these reactions are short, comprising only a few nucleotides. Indeed supplementing such reactions with additional (non-radiolabeled) UTP leads to the generation of longer U-tails (Figure 3a, compare lanes 1, 2, and 3). Interestingly, addition of Dis3l2 leads to the selective degradation of the pre-let-7 with longer U-tails (Figure 3a). These data define the minimal set of proteins and enzymes required to recapitulate the selective degradation of pre-let-7 observed in vivo, and raise questions regarding U-tail length requirements to stimulate Dis3l2-mediated degradation. To address this we prepared a panel of pre-let-7 RNA substrates with varying U-tail lengths and monitored Dis3l2 degradation activity. Tails of at least 10 uridines were found to stimulate Dis3l2 activity with maximal stimulation observed with U-tails of 14 or greater. This result is consistent with the average length the U-tail found on pre-let-7 RNAs cloned and sequenced from Lin28-expressing cells[5].

To examine the Dis3l2 domain requirements we generated three deletion mutants lacking either the N-terminus, C-terminus, or both N and C-terminal regions (Figure 3d). RNA degradation assays and electromobility shift assays (EMSA) revealed that truncation of either the N- or the C-terminus region abrogated both Dis3l2 binding and nuclease activities on uridylated pre-let-7 RNA (Figures 3d–e). This suggests that both the cold-shock domain(s) as well as the S1 domain are required for binding to uridylated pre-let-7. Though the catalytic mutant (D389N) Dis3l2 was inactive in RNA degradation assays it retained the ability to selectively bind to uridylated pre-let-7 (Figure 3e and Supplementary Figure 4b). RNA degradation and binding assays using an unrelated RNA, pre-miR-21−/+14U, established the sufficiency of an oligo-U tail serving as a signal to trigger Dis3l2-mediated decay (Supplementary Figure 4c–d).

To examine the role of Dis3l2 in the let-7 pathway we used siRNAs to deplete Lin28A, Zcchc11, or Dis3l2 expression in mouse ESCs. We also included siRNAs that target a related family member Dis3l1 (Figure 4a–b). We monitored effects of gene knockdown on mature miRNA expression by q.RT-PCR and Northern blot (Figure 4c–d). While Lin28A knockdown caused the expected accumulation of multiple let-7 miRNAs, knockdown of Dis3l2 (or Dis3l1) had no effect. We did however observe a modest increase in let-7 expression in the Zcchc11-depleted samples as previously reported[3–5]. Uridylated pre-let-7 has been previously shown to be resistant to cleavage by affinity-purified Dicer complex(es) and consistently we found pre-let-7+14U to be a poor substrate for recombinant Dicer in processing assays. In comparison pre-let-7 was processed by Dicer to ~22 nt duplexes (Figure 4e). Considering that pre-let-7+14U is inefficiently processed by Dicer we postulated that knockdown of Dis3l2 in cells could lead to accumulation of uridylated pre-let-7 without affecting levels of mature let-7. To test this we developed a sensitive q.RT-PCR-based assay for the specific detection of uridylated pre-let-7. We used an oligo-dA

primer for the reverse transcriptase first-strand cDNA synthesis step and used primers complementary to pre-let-7 for detection of uridylated pre-let-7 by real-time PCR. This approach allowed us to specifically detect uridylated pre-let-7 (Supplementary Figure 6a). RNA from the knockdown samples was size fractionated to specifically measure relative levels of uridylated pre-let-7 in the <200nt fraction and the corresponding pri-let-7 transcripts in the large >200nt fraction. This revealed the specific accumulation of uridylated pre-let-7a-1 and pre-let-7g upon Dis3l2 knockdown (Figure 4f), whereas levels of the corresponding pri-let-7 transcripts were unchanged (Figure 4g). PCR products were cloned and sequenced to confirm the specificity of this assay (Supplementary Figure 6b–c). Similar results were found using stable Dis3l2 knockdown ESCs (Supplementary Figure 7a–e). To further confirm the role of Dis3l2 in the regulation of uridylated pre-let-7 levels we performed Northern blot using a probe complementary to the terminal loop region of let-7g. This revealed a slower-migrating pre-let-7 band upon Dis3l2 depletion that likely corresponds to oligouridylated pre-let-7 (Figures 4h–i). Finally we individually depleted two additional 3′-5′ exonucleases, Exosc10 (RRP6) and Rrp44 (Dis3) from ESCs and measured relative pre-let-7 levels by q.RT-PCR. Knockdown of these exosome-associated nucleases did not affect uridylated pre-let-7 levels (Supplementary Figure 8). These results provide strong support that Dis3l2 is the downstream nuclease that mediates the decay of uridylated pre-let-7 in the Lin28 pathway.

Our results identify Dis3l2 as a new component of the Lin28/let-7 pathway as the downstream nuclease responsible for the decay of uridylated pre-let-7 (Supplementary Figure 9). This contention is based on the following: First, Dis3l2 specifically associates with uridylated pre-let-7 in RNA affinity-purifications and is detected as a component of a Lin28A-containing ribonucleoprotein complex(es). Second, purified Dis3l2 (but not catalytically inactive mutant Dis3l2) complexes display substrate preference for uridylated pre-let-7 in RNA degradation assays in vitro. Third, in vitro reconstitution experiments with recombinant Dis3l2 reveal the sufficiency of this enzyme for the preferential degradation of uridylated pre-let-7. Last, knockdown of Dis3l2 causes the specific accumulation of uridylated pre-let-7 in mouse ESCs.

Dis3l2 belongs to a family of related 3′-5′ exonucleases with similar domain organization to bacterial RNase II[6,21,22]. Interestingly germline mutations in the Dis3l2 gene were recently found to be responsible for Perlman syndrome, a rare, autosomal recessive, fetal overgrowth syndrome[6]. In addition to being large, affected individuals are hypotonic, have organomegally, characteristic facial dysmorphism, renal abnormalities, neurodevelopmental problems, and a dramatically high susceptibility Wilms' tumors (Nephroblastoma) with >60% of surviving children developing Wilms' tumors. Moreover Dis3l2 was found to be mutated in ~30% of sporadic Wilms' tumors analyzed[6]. It will be important to explain the role of Dis3l2 in the genesis and development of Perlman syndrome and Wilms' tumors. Future experiments with knockout mouse models will shed light on question. Our work uncovers the first physiologic RNA substrate of Dis3l2. Considering the similarities between the disease phenotypes associated with Dis3l2 deletion and those caused by Lin28 gain-of-function (i.e. overgrowth and tumorigenesis) it is tempting to speculate that this novel role of Dis3l2 in the Lin28-let-7 pathway is relevant to Perlman syndrome and cancer.

Our identification of a decay pathway for uridylated RNAs raises questions about how widespread this type of regulation might be on a transcriptome scale as well as the mechanism by which oligouridylation promotes Dis3l2 ribonucleolytic activity. So far there are few known examples where 3′ uridylation can serve as a decay signal; these include histone mRNA regulation during the mammalian cell cycle, and the widespread uridylation-dependent mRNA decapping and decay in *Schizosaccharomyces pombe* [23–25]. This model has analogies with other systems; for example 3′-5′ RNA decay in *E. coli* by the

'Degradosome' is stimulated by short poly(A) tails[26,27]. Similarly in *Saccharomyces cerevisiae* the Trf4/Air2/Mtr4 polyadenylation (TRAMP) complex catalyzes the addition of oligoA-tail that promotes 3′-5′ RNA decay by the exosome as part of a nuclear RNA surveillance mechanism[28,29]. In the case of pre-let-7 the 3′ oligouridylation has two consequences; 1) to block Dicer processing, and 2) to stimulate decay by Dis3l2, therefore even though Dis3l2 displays relatively modest substrate preference for uridylated pre-let-7 in vitro, the two-step mechanism safeguards against the production of mature let-7 miRNA.

METHODS SUMMARY

Affinity pull-down assays

Synthetic pre-let-7a-1 or pre-let-7a-1+14U was conjugated to agarose beads and incubated with whole-cell extract from P19 cells. Affinity eluate was subjected to SDS-PAGE and Coomassie blue staining. Bands were excised and subjected to mass spectroscopic sequencing. Protein complexes were affinity-purified using α-Flag M2 agarose beads (Sigma).

Plasmids and cDNA cloning

Dis3l2 cDNA was cloned into pFlag-CMV2 (Sigma). Dis3l2 D389N was generated by site-directed mutagenesis. cDNA was subcloned into pETDuet-1 for His-tagged Dis3l2 expression.

Recombinant Dis3l2 protein purification

Ni-NTA beads were used for the purification of His-Dis3l2 from IPTG induced BL21-CodonPlus® competent bacteria (Stratagene).

RNA degradation assays

RNA degradation assays were performed using either 5′ end-labeled synthetic pre-miRNA or uniformly labeled in vitro transcribed pre-miRNA together with Dis3l2 in RNA degradation buffer and incubated at 37°C.

RNA Electromobility shift assays (EMSA)

EMSA experiments were performed as described previously[16]. Nucleoprotein complexes were resolved by 4–20% non-denaturing TBE gel electrophoresis and visualized by autoradiography.

Transfections and siRNA/shRNA knockdowns

All transfections were performed with Lipofectamine (Invitrogen) per manufacturer's instructions. Lentivirus production, infection, and stable cell selection are as described [17].

Quantitative RT-PCR

RNA was isolated using TRIzol reagent (Invitrogen) and size fractionated using mirVana™ miRNA isolation (Ambion). For detection of uridylated pre-miRNA, 1 μg (<200 nt RNA fraction) was treated with DNase then reverse transcribed using oligo$(dA)_{12}$ primer and SuperScript III (Invitrogen). Q.RT-PCR was performed using iQ SYBR Green Supermix (Bio-Rad).

Northern blotting

10 μg total RNA from each sample was used for Northern blotting as previously described[19].

Dicer assays

Recombinant Flag-Dicer Protein was purified from insect cells as previously described [19].

METHODS

Cell culture

HEK293 cells were maintained in DMEM, P19 cells in MEMα+GlutaMax™-1, and ESCs in DMEM with ESGRO (1,000 units/ml), supplemented with antibiotics, and 10% (for HEK293, P19) or 15% (for ESC) fetal bovine serum. A Dox-inducible Flag-Lin28A ESC line was used [3,12]. The MISSION® shRNA plasmid DNA (Sigma, TRC number TRCN0000120760 for shRNA#1 and TRCN0000120761 for shRNA#2, TRCN0000120745 for Dis3 shRNA, or TRCN0000123544 for Exosc10 shRNA) together with pLP1, pLP2, and VSVG were transfected into 293T cells to produce lentiviral particles that were used to infect V6.5 ESCs. The Dis3l2 shRNA stable cells were then created by puromycin (2.5 μg/ml) selection.

Affinity pull-down assays

For RNA affinity pull-down, synthetic mmu-pre-let-7a-1 or mmu-pre-let-7a-1+14U was conjugated to adipic acid dihydrazide agarose beads and incubated with whole-cell extract from P19 cells [8]. The affinity eluate was subjected to SDS–polyacrylamide gel electrophoresis (SDS-PAGE) followed by Coomassie blue staining using the Colloidal Blue Staining Kit' (Life Technologies™). Bands were excised, and subjected to mass spectroscopic sequencing. The sequencing results were further confirmed by Western blotting. For affinity purification of Flag-Lin28A, KH2 ESCs were treated with Dox at 6 μg/ml for 48 hours and then harvested in the lysis buffer (20 mM Tris-HCl, pH 8.0, 137 mM NaCl, 1 mM EDTA, 1% (v/v) Triton X-100, 10% (v/v) Glycerol, 1.5 mM $MgCl_2$, 1 mM DTT, 0.2 mM PMSF) supplemented with 40 units/ml of RNase inhibitor (rRNasin, Promega). Protein complexes were affinity-purified using α-Flag M2 agarose beads (Sigma). Beads were extensively washed with lysis buffer for a total of seven times before elution with 0.5 mg/ml Flag peptide. The eluates were analyzed by SDS-PAGE and Western blotting.

Mass spectrometry

The mass spectrometric protein analysis was performed at the Proteomics Center at Boston Children's Hospital. Bands of interest were excised from the Coomassie-stained SDS-PAGE gel, washed with a 2:1 ratio of 100mM ammonium bicarbonate and acetonitrile, reduced with 10 mM DTT at 56°C for 45 minutes and alkylated for 30 minutes at room temperature, in the dark, with 55mM Iodoacetamide. Samples were digested with sequencing grade trypsin (Promega) at a concentration of 12.5ng/ul in 100mM ammonium bicarbonate at 37°C overnight. Peptides were extracted with 100mM ammonium bicarbonate and acetonitrile, and then dried in a speedvac. Samples were resuspended in 5 % acetonitrile and 5 % formic acid before direct injection into the LC/MS system comprising of a nanoLC AS-2 autosampler, a nanoLC 2D HPLC pump (both Eksigent, Dublin, CA), and an LTQ mass spectrometer (Thermo Scientific, San Jose, CA). The LC-system for the mass spectrometer featured an reversed phase column in-house packed into PicoTip Emitters (New Objective, Woburn, MA) using Magic C18 (3 um, 200 Å; Michrom Bioresource) packing material. The peptides were eluted with a 30 min linear gradient and data was acquired in a data dependent fashion, i.e. the 6 most abundant species were selected for fragmentation by collision induced dissociation. The .raw files were converted into .mgf files using in-house written scripts[30]. For each fragment ion spectrum, only the 200 most intense fragment ions were exported into the mgf file. The mass spectrometric data was

searched against Uniprot-Mouse database using the protein identification software Protein Pilot. The results were then filtered to include only proteins with a global FDR of 1%.

Plasmids and DNA cloning

Dis3l2 cDNA was generated by PCR using the forward (5′-aagcttgcggccgcgAACCATCCTGACTACAAGCTGAACCTTCGG-3′) and the reverse (5′-agacctagtcgacTCAGTCCTCAGGCTCCTCATCAGACGCC-3′) primers, and was cloned into the NotI and SalI sites of pFlag-CMV2 (Sigma). For generating Dis3l2 D389N mutant, site-directed mutagenesis was performed using the forward (5′-CTGCTCGCGACCTTAATGATGCCCTCGC-3′) and the reverse (5′-GCGAGGGCATCATTAAGGTCGCGAGCAG-3′) primers. For generating Histagged Dis3l2, PCR product from the forward (5′-actaggaattcgAACCATCCTGACTACAAGCTGAACCTTCGG-3′) and the reverse (5′-aagcttgcggccgcTCAGTCCTCAGGCTCCTCATCAGACGCC-3′) primers was cloned into the EcoRI and NotI sites of pETDuet-1. For CT-GFP and NT-GFP fusions, the GFP Fusion TOPO TA expression kits (Invitrogen) were used. For CT-GFP fusions, the forward (5′-ACC ATG AAC CAT CCT GAC TAC AAG CTG AAC-3′) and the reverse (5′-CGT CCT CAG GCT CCT CAT CAG-3′) primers were used. For NT-GFP fusions, the forward (5′-AAC CAT CCT GAC TAC AAG CTG AAC-3′) and the reverse (5′-TCA GTC CTC AGG CTC CTC ATC AG-3′) primers were used. For deletion mutants, Dis3l2 truncated cDNA were amplified by PCR with the forward (5′-AAC AAG CGG CCG CGA ACC ATC CTG ACT ACA AGC TGA ACC-3′) and the reverse (5′-AAC AAG AAT TGA GTA GCC CAG AGC AGC AGC-3′) primers to generate the C-terminus deletion mutant, with the forward (5′-AAC AAG CGG CCG CGA GAA GAG ACC TAA GGA AAG ACT GTA TCT TCA C-3′) and the reverse (5′-AAC AAG AAT TCA GTC CTC AGG CTC CTC ATC-3′) primers to generate the N-terminus deletion and with the forward (5′-AAC AAG CGG CCG CGA GAA GAG ACC TAA GGA AAG ACT GTA TCT TCA C-3′) and the reverse (5′-AAC AAG AAT TGA GTA GCC CAG AGC AGC AGC-3′) primers to generate the N and C-terminus deletion. These PCR products were cloned into NotI and EcoRI sites of pFLAG-CMV2 vector (Sigma). Flag-TRBP and Flag-Trim71 constructs were as described[15,19].

Recombinant Dis3l2 protein purification

Transformed BL21-CodonPlus® Competent bacteria (Stratagene) were grown to an OD600nm of 0.4–0.6. Expression was induced 100μM IPTG for 2–3 hours. Cell pellets were resuspended in cold lysis buffer [20mM imidazole pH 8.0 in PBS, 0.1% Phenylmethyl sulfonyl fluoride (PMSF)] and sonicated. Cleared lysates were incubated with Ni-NTA beads and after 90 minutes incubation at 4°C the beads were washed with 80 column volumes wash buffer [10mM Tris (pH 7.8), 50mM imidazole pH 8.0, 500mM NaCl, 0.1% PMSF). Bound His-tagged proteins were eluted from the column with 1 volume elution buffer [10mM Tris (pH 7.8), 500mM imidazole pH 8.0, 500mM NaCl, 0.1% fresh PMSF] and dialyzed overnight against BC100 [20 mM Tris-HCl (pH 7.8), 100 mM KCl, 0.2 mM EDTA, 10% glycerol]. Purified protein was dialyzed against RNA degradation buffer (see below) and supplemented with 20% glycerol before storage at −80°C. For affinity purification of ectopically expressed FLAG-Lin28A or FLAG-Lin28A W46A, V6.5 ESC were transfected using Lipofectamine 2000 (Invitrogen) and collected 48 hours later. Cells were lysed as described above, except for the addition of RNase A (20 mg/ml final, QIAGEN) where indicated.

RNA degradation assays

RNA degradation assays were performed in a total of 20 μl reaction using 6.25 nM 5′ end-labeled pre-miR-21, pre-let-7a-1, or pre-let-7a-1+14U RNA (see Table 2) together with Dis3l2 and/or Lin28A. The reactions were set up in the RNA degradation buffer (20 mM

HEPES-KOH pH 7.5, 50 mM KCl, 0.05 mM $MgCl_2$, 1 mM DTT) and incubated at 37°C for 90 minutes. For time-course assays; recombinant 6x-His Dis3l2 was incubated with radiolabeled pre-let-7a-1 or pre-let-7a-1+14U. Bands from three independent experiments were quantified using ImageJ (NIH) and plotted using Prism (Graphpad). Values were fitted to one-phase decay curves with error bars representing +/− s.d. (n=3). For Uridylation-stimulated degradation assays; i*n vitro* uridylation assays were performed as described previously [3,4,16] except with the addition of 10μM cold competitor uridine triphosphate and immunopurified Dis3l2 where indicated.

In vitro transcription of pre-miRNAs

In vitro transcribed pre-let-7 RNAs were generated as substrates RNA degradation assays (in Figure 3b). DNA templates for in vitro transcription of pre-let-7 with different 3′ ends by PCR amplification using were generated using a universal 5′-primer (acggttcagcTAATACGACTCACTATAGGGTGAGGTAGTAGTTTGTACAGTTTGAGG) (T7 promoter sequence underlined) and a 3′-primer listed in the Table 1 to amplify from a plasmid DNA template containing pri-let-7[8]. PCR products were cloned and sequence verified. DNA templates (PCR products) were gel-purified and in vitro transcription was performed according to Riboprobe *in-vitro* transcription systems using a-^{32}P rGTP and T7 RNA polymerase (Promega). The labeled pre-miRNAs were treated with RQ1 DNase and cleaned by illustra MicroSpin G-25 Column (GE Healthcare Life Sciences).

RNA Electromobility shift assays (EMSA)

EMSA experiments were performed as described previously[16]. Briefly, 1nM of the indicated radiolabeled synthetic RNA was incubated in the binding buffer (50 mM Tris pH 7.6, 100mM NaCl, 10 mM β-Mercaptoethanol, 1 unit/μl RNaseOUT) with varying concentrations of catalytically inert recombinant 6x-His Dis3L2 or recombinant 6x-His Lin28 in the absence of competitor RNA. Nucleoprotein complexes were resolved by 4–20% non-denaturing TBE gel electrophoresis (Biorad, #345-0059) and visualized by autoradiography.

Antibodies and synthetic RNA

Transfections and siRNA/shRNA knockdowns

All transfections were performed with Lipofectamine (Invitrogen) per manufacturer's instructions. The sequences of the shRNA hairpins and siRNAs are listed in Table 3. Lentivirus production, infection, and stable cell selection are as described [17].

mRNA and miRNA quantitative RT-PCR

Total RNA was isolated using TRIzol reagent (Invitrogen). For fractionation of less than 200 nucleotides (nt) long RNA, total RNA was processed by mirVana™ miRNA Isolation Kit according to the manufacturer's instructions (Cat# AM1560, Ambion). For mRNA, 100 ng of total RNA was reverse transcribed using random hexamers and SuperScript III (Invitrogen). For mature miRNA, 10 ng of total RNA was reverse transcribed using gene-specific stem-loop RT primers and Multiscribe reverse transcriptase (Applied Biosystems). For pre-miRNA, 1 μg of less than 200 nt fractionated RNA was first treated with 0.66 unit of RNase-free DNase (Promega) (60 min at 37°C), stopped with 1 mM of EDTA (10 min at 65°C), and reverse transcribed by oligo$(dA)_{12}$ (60 min at 50°C) using SuperScript III (Invitrogen). The resulting cDNA was further digested with RNase H (30 min at 37°C). For mRNA and pre-miRNA, iQ SYBR Green Supermix (Bio-Rad) was used for quantitating the cDNA. For mature-miRNA, TaqMan Universal PCR Master Mix, No AmpErase UNG (Applied Biosystems) was used for cDNA detection. All quantitative PCR were performed using iCycler iQ Multicolor Real-Time PCR Detection System (Bio-Rad). Normalization

controls include ACTB for mRNAs as well as for primiRNAs, U6 for pre-miRNA, and snoRNA142 for mature miRNAs. For all RT-PCRs, minus reverse transcriptase (-RT) and water control samples were included and in all cases the signals were undetectable (data not shown). The primer sequences used in this study are listed in Table 4.

Northern blotting

10 μg total RNA from each sample was used for Northern blotting as previously described[19]. Probe sequences for detecting precursor and mature miRNA are as follows: 5′-TATCTCCTGTACCGGGTGGTATCATAGACCCTCA-3′ for pre-let-7g; 5′-AACTATACAACCTACTACCTCA-3′ for let-7a; 5′-AACTGTACAAACTACTACCTCA-3′ for let-7g.

Dicer assays

Recombinant Flag-Dicer Protein was purified from insect cells as previously described [19]. Dicer processing of pre-let-7 or pre-let-7+14U was performed by incubating recombinant Dicer with gel-purified 5′-end labeled synthetic pre-miRNA in a buffer containing 3.2 mM MgCl2, 20 mMTris-HCl (pH 7.9), 0.1M KCl, 10% glycerol, 5 mM DTT, 0.2 mM PMSF, 40 units/ml of RNase inhibitor (RNasin, Promega) for 1 h at 37°C. Samples were resolved by 15% denaturing polyacrylamide gel.

Supplementary Material

Refer to Web version on PubMed Central for supplementary material.

Acknowledgments

We thank Robert LaPierre for technical assistance and Dr. Fei-Long Meng for Rrp44 and Exosc10 shRNA. Thanks to Children's Hospital Boston/IDDRC Proteomics Core for mass spectromety. R.I.G was supported by grants from the US National Institute of General Medical Sciences (NIGMS) (R01GM086386) and The American Cancer Society (121635-RSG-11-175-01-RMC). J.E.T. was supported by a pre-doctoral fellowship from the National Science Foundation. R.T. was supported by a fellowship from Boston Children's Hospital.

References

1. Thornton JE, Gregory RI. How does Lin28 let-7 control development and disease? Trends Cell Biol. 2012; 22:474–482. S0962-8924(12)00104-3 [pii]. 10.1016/j.tcb.2012.06.001 [PubMed: 22784697]
2. Heo I, et al. TUT4 in concert with Lin28 suppresses microRNA biogenesis through pre-microRNA uridylation. Cell. 2009; 138:696–708. S0092-8674(09)00964-7 [pii]. 10.1016/j.cell.2009.08.002 [PubMed: 19703396]
3. Hagan JP, Piskounova E, Gregory RI. Lin28 recruits the TUTase Zcchc11 to inhibit let-7 maturation in mouse embryonic stem cells. Nat Struct Mol Biol. 2009; 16:1021–1025. nsmb.1676 [pii]. 10.1038/nsmb.1676 [PubMed: 19713958]
4. Thornton JE, Chang HM, Piskounova E, Gregory RI. Lin28-mediated control of let-7 microRNA expression by alternative TUTases Zcchc11 (TUT4) and Zcchc6 (TUT7). RNA. 2012; 18:1875–1885. rna.034538.112 [pii]. 10.1261/rna.034538.112 [PubMed: 22898984]
5. Heo I, et al. Lin28 mediates the terminal uridylation of let-7 precursor MicroRNA. Mol Cell. 2008; 32:276–284. S1097-2765(08)00660-6 [pii]. 10.1016/j.molcel.2008.09.014 [PubMed: 18951094]
6. Astuti D, et al. Germline mutations in DIS3L2 cause the Perlman syndrome of overgrowth and Wilms tumor susceptibility. Nat Genet. 2012; 44:277–284. ng.1071 [pii]. 10.1038/ng.1071 [PubMed: 22306653]
7. Roush S, Slack FJ. The let-7 family of microRNAs. Trends Cell Biol. 2008; 18:505–516. [PubMed: 18774294]
8. Viswanathan SR, Daley GQ, Gregory RI. Selective blockade of microRNA processing by Lin28. Science. 2008; 320:97–100. 1154040 [pii]. 10.1126/science.1154040 [PubMed: 18292307]

9. Newman MA, Thomson JM, Hammond SM. Lin-28 interaction with the Let-7 precursor loop mediates regulated microRNA processing. RNA. 2008; 14:1539–1549. rna.1155108 [pii]. 10.1261/rna.1155108 [PubMed: 18566191]
10. Rybak A, et al. A feedback loop comprising lin-28 and let-7 controls pre-let-7 maturation during neural stem-cell commitment. Nat Cell Biol. 2008; 10:987–993. ncb1759 [pii]. 10.1038/ncb1759 [PubMed: 18604195]
11. Ambros V, Horvitz HR. Heterochronic mutants of the nematode Caenorhabditis elegans. Science. 1984; 226:409–416. [PubMed: 6494891]
12. Zhu H, et al. Lin28a transgenic mice manifest size and puberty phenotypes identified in human genetic association studies. Nat Genet. 2010; 42:626–630. ng.593 [pii]. 10.1038/ng.593 [PubMed: 20512147]
13. Zhu H, et al. The Lin28/let-7 axis regulates glucose metabolism. Cell. 2011; 147:81–94. S0092-8674(11)01003-8 [pii]. 10.1016/j.cell.2011.08.033 [PubMed: 21962509]
14. Yu J, et al. Induced pluripotent stem cell lines derived from human somatic cells. Science. 2007; 318:1917–1920. 1151526 [pii]. 10.1126/science.1151526 [PubMed: 18029452]
15. Chang HM, et al. Trim71 cooperates with microRNAs to repress Cdkn1a expression and promote embryonic stem cell proliferation. Nat Commun. 2012; 3:923. ncomms1909 [pii]. 10.1038/ncomms1909 [PubMed: 22735451]
16. Piskounova E, et al. Lin28A and Lin28B Inhibit let-7 MicroRNA Biogenesis by Distinct Mechanisms. Cell. 2011; 147:1066–1079. S0092-8674(11)01289-X [pii]. 10.1016/j.cell.2011.10.039 [PubMed: 22118463]
17. Viswanathan SR, et al. Lin28 promotes transformation and is associated with advanced human malignancies. Nat Genet. 2009; 41:843–848. [PubMed: 19483683]
18. Nam Y, Chen C, Gregory RI, Chou JJ, Sliz P. Molecular Basis for Interaction of let-7 MicroRNAs with Lin28. Cell. 2011; 147:1080–1091. S0092-8674(11)01266-9 [pii]. 10.1016/j.cell.2011.10.020 [PubMed: 22078496]
19. Chendrimada TP, et al. TRBP recruits the Dicer complex to Ago2 for microRNA processing and gene silencing. Nature. 2005; 436:740–744. nature03868 [pii]. 10.1038/nature03868 [PubMed: 15973356]
20. Dziembowski A, Lorentzen E, Conti E, Seraphin B. A single subunit, Dis3, is essentially responsible for yeast exosome core activity. Nat Struct Mol Biol. 2007; 14:15–22. nsmb1184 [pii]. 10.1038/nsmb1184 [PubMed: 17173052]
21. Tomecki R, et al. The human core exosome interacts with differentially localized processive RNases: hDIS3 and hDIS3L. EMBO J. 2010; 29:2342–2357. emboj2010121 [pii]. 10.1038/emboj.2010.121 [PubMed: 20531386]
22. Staals RH, et al. Dis3-like 1: a novel exoribonuclease associated with the human exosome. EMBO J. 2010; 29:2358–2367. emboj2010122 [pii]. 10.1038/emboj.2010.122 [PubMed: 20531389]
23. Mullen TE, Marzluff WF. Degradation of histone mRNA requires oligouridylation followed by decapping and simultaneous degradation of the mRNA both 5′ to 3′ and 3′ to 5′. Genes Dev. 2008; 22:50–65. 22/1/50 [pii]. 10.1101/gad.1622708 [PubMed: 18172165]
24. Norbury CJ. 3′ Uridylation and the regulation of RNA function in the cytoplasm. Biochem Soc Trans. 2010; 38:1150–1153. BST0381150 [pii]. 10.1042/BST0381150 [PubMed: 20659020]
25. Rissland OS, Norbury CJ. Decapping is preceded by 3′ uridylation in a novel pathway of bulk mRNA turnover. Nat Struct Mol Biol. 2009; 16:616–623. nsmb.1601 [pii]. 10.1038/nsmb.1601 [PubMed: 19430462]
26. Carpousis AJ, Vanzo NF, Raynal LC. mRNA degradation. A tale of poly(A) and multiprotein machines. Trends Genet. 1999; 15:24–28. S0168-9525(98)01627-8 [pii]. [PubMed: 10087930]
27. Blum E, Carpousis AJ, Higgins CF. Polyadenylation promotes degradation of 3′-structured RNA by the Escherichia coli mRNA degradosome in vitro. J Biol Chem. 1999; 274:4009–4016. [PubMed: 9933592]
28. LaCava J, et al. RNA degradation by the exosome is promoted by a nuclear polyadenylation complex. Cell. 2005; 121:713–724. S0092-8674(05)00442-3 [pii]. 10.1016/j.cell.2005.04.029 [PubMed: 15935758]

29. Wyers F, et al. Cryptic pol II transcripts are degraded by a nuclear quality control pathway involving a new poly(A) polymerase. Cell. 2005; 121:725–737. S0092-8674(05)00443-5 [pii]. 10.1016/j.cell.2005.04.030 [PubMed: 15935759]

30. Renard BY, et al. When less can yield more - Computational preprocessing of MS/MS spectra for peptide identification. Proteomics. 2009; 9:4978–4984.10.1002/pmic.200900326 [PubMed: 19743429]

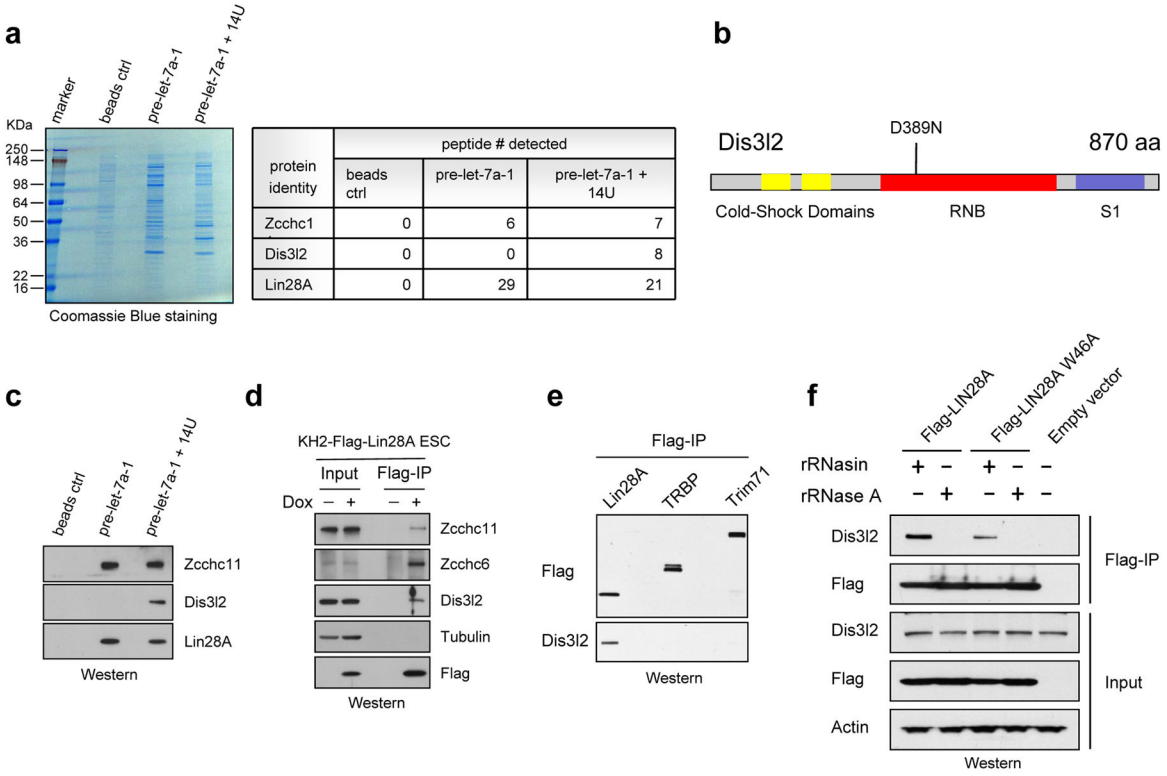

protein identity	peptide # detected		
	beads ctrl	pre-let-7a-1	pre-let-7a-1 + 14U
Zcchc1	0	6	7
Dis3l2	0	0	8
Lin28A	0	29	21

Figure 1. Dis3l2 is associated with uridylated pre-let-7

(a) Affinity-purified proteins analyzed by Coomassie blue staining and mass spectrometry. **(b)** Diagrammatic representation of Dis3l2 protein, Accession number (NCBI): NP_001165628.1. Cold-shock domains, Ribonuclease II domain (RNB), and S1 RNA-binding domain are indicated. aa, amino acids. The mutated catalytic Aspartic Acid is indicated. **(c)** Western blotting analysis of samples in (a) with indicated antibodies. **(d–f)** co-IP and Western blot analyses.

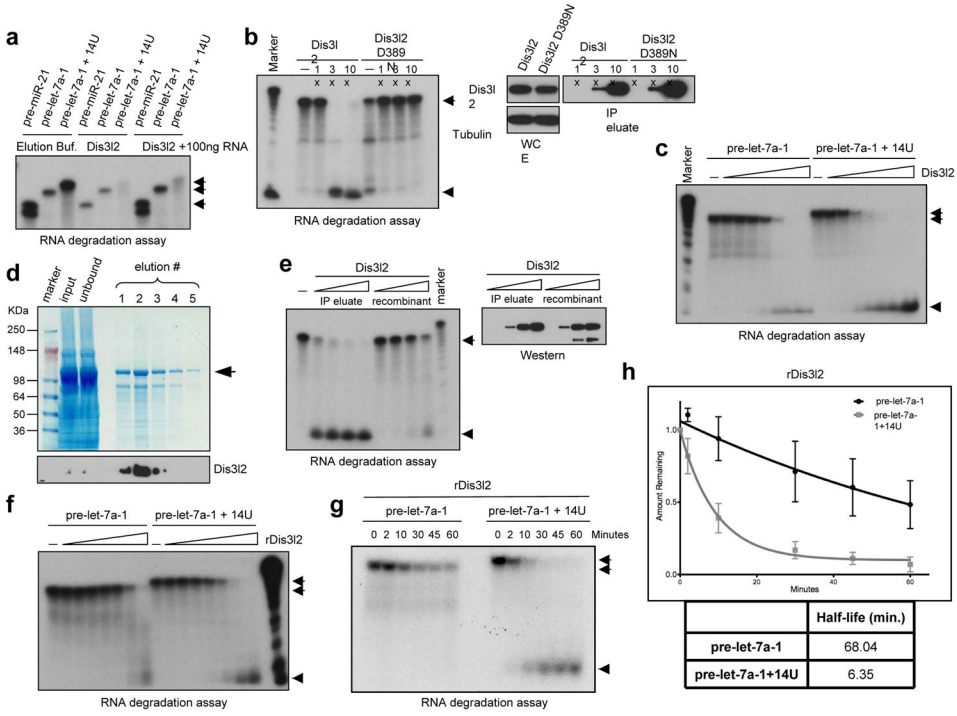

Figure 2. Dis3l2 preferentially degrades uridylated pre-let-7

(a) Flag-Dis3l2 incubated with different radiolabeled pre-miRNAs. Where indicated, 100ng competitor RNA was added to reduce background activity. **(b)** Flag-tagged Dis3l2 or mutant Dis3l2 incubated with pre-let-7a-1+14U **(c)** RNA degradation assay with a titration of Flag-Dis3l2. **(d)** His-Dis3l2 examined by Coomassie blue staining and Western blot. **(e)** Flag-Dis3l2 and His-Dis3l2 analyzed by Western blot and activity. **(f)** RNA degradation assay with a titration of His-Dis3l2. **(g)** Representative time course assay. **(h)** Quantitation of three independent experiments as in (g) with the corresponding calculated RNA half-lives. $p<0.01$ [two-way analysis of variance (ANOVA) test]. Arrows indicate radiolabeled pre-miRNA while arrowheads indicate degradation products.

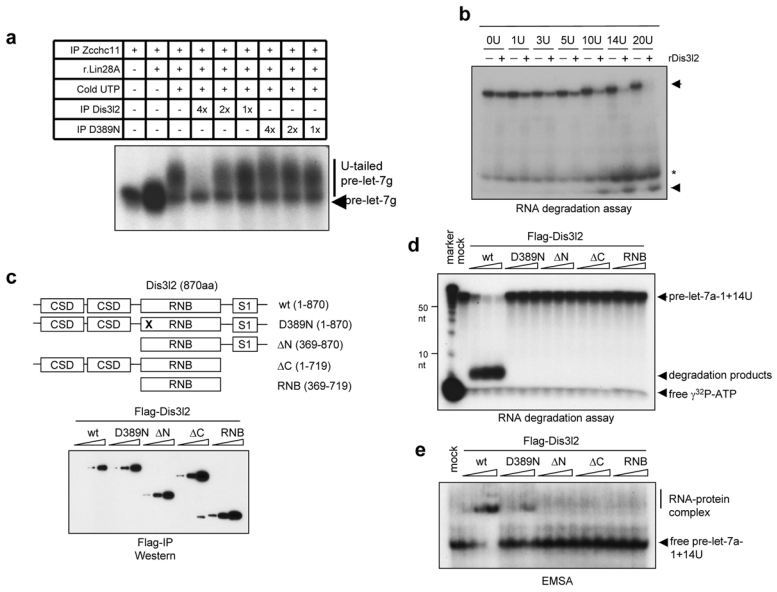

Figure 3. Molecular determinants of Disl32 activity

(a) Reconstitution assays reveal longer Flag-uridine tails are preferred substrates for Dis3l2. **(b)** RNA degradation assays with in vitro transcribed pre-let-7 RNAs with indicated 3′ U-tail. **(c)** Schematic representation and Western blot of different Dis3l2 truncations used for **(d)** RNA degradation assays and **(e)** EMSA.

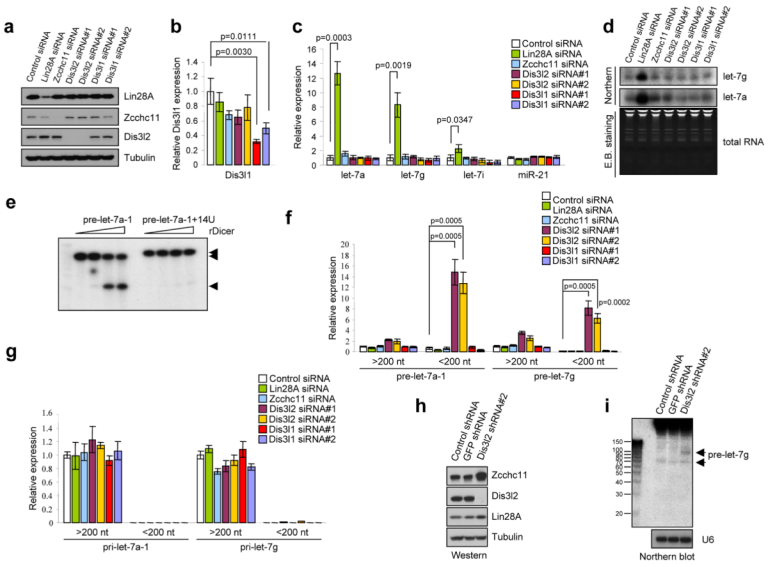

Figure 4. Dis3l2 is required for degradation of uridylated pre-let-7 in embryonic stem cells

(a) Western blot analysis of siRNA knockdown. **(b)** quantitative RT-PCR (q.RT-PCR) analysis of Dis3l1 knockdown. Error bars ±S.D. (n=3). **(c)** mature miRNA levels measured by q.RT-PCR. Error bars ±S.D. (n=3) and **(d)** Northern blot. **(e)** Dicer processing assay with Arrows indicating pre-miRNA and arrowhead indicating Dicer products. **(f)(g)** 1 μg of total RNA from the samples in (a) was fractionated into >200 nt and <200 nt long RNA and relative levels of pre-let-7 (f) or pri-let-7 (g) RNA were quantitated by real-time PCR. Error bars ±S.D. (n=3). **(h)** Western blot analysis of Dis3l2 cells. **(i)** Northern blot analysis of pre-let-7g.

Table 1

pre-let-7g-$(U)_n$	3′-primer
pre-let-7g-0U	GCAAGGCAGTGGCCTGTACAGTTATC
pre-let-7g-1U	aGCAAGGCAGTGGCCTGTACAGTTATC
pre-let-7g-3U	aaaGCAAGGCAGTGGCCTGTACAGTTATC
pre-let-7g-5U	aaaaaGCAAGGCAGTGGCCTGTACAGTTATC
pre-let-7g-10U	aaaaaaaaaaGCAAGGCAGTGGCCTGTACAGTTATC
pre-let-7g-14U	aaaaaaaaaaaaaaGCAAGGCAGTGGCCTGTACAGTTATC
pre-let-7g-20U	aaaaaaaaaaaaaaaaaaaaGCAAGGCAGTGGCCTGTACAGTTATC
pre-miR-21 forward	acggttcagcTAATACGACTCACTATAGGGTAGCTTATCAGACTGATGTTGACTG
pre-miR-21 reverse	GACAGCCCATCGACTGCTGTTG
pre-miR-21-14U reverse	aaaaaaaaaaaaaaGACAGCCCATCGACTGCTGT

Table 2

Antibodies and the working concentrations

Antibody	Cat. #	Source	Conc. used
α-Dis3l2	NBP1-84740	Novus Biologicals	0.4 μg/ml
α-Zcchc11	18980-1-AP	ProteinTech Group	1:1,000
α-Zcchc6	Custom-made	Open Biosystems	1:500
α-Rrp44	Cat #14689-1-AP	ProteinTech Group	1:1000
α-Exosc10	Cat # ab50558	Abcam	1 μg/ml
α-Lin28A (A177)	#3978	Cell Signaling	1:1,000

Table 3

The synthetic RNA sequences

RNA	Cat. #	Source	Sequence
mmu-pre-let-7a-1	N/A	Dharmacon	UGAGGUAGUAGGUUGUAUAGUUUUAGGGUCACACCCACCACUGGGAGAUAACUAUACAAUCUACUG
mmu-pre-let-7a-1+14U	N/A	Dharmacon	UGAGGUAGUAGGUUGUAUAGUUUUAGGGUCACACCCACCACUGGGAGAUAACUAUACAAUCUACUG
mmu-pre-miR-21	N/A	Dharmacon	UAGCUUAUCAGACUGAUGUUGACUGUUGAAUCUCAUGGCAACAGCAGUCGAUGGGCUGUC
control siRNA #1	D-001810-01	Dharmacon	UGGUUUACAUGUCGACUAA
control siRNA #2	D-001810-02	Dharmacon	UGGUUUACAUGUUGUGUGA
Lin28A siRNA	Custom	Dharmacon	GGGUUGUGAUGACAGGCAA
Zcchc11 siRNA	J-065226-06	Dharmacon	GGGCUAAGCUGUGCUAUAU
mouse Dis3l2 siRNA#1	J-054755-10	Dharmacon	CCGCUUUGCUGACGUCAUA
mouse Dis3l2 siRNA#2	J-054755-11	Dharmacon	GAAUUUACGUACCUCUCAA
mouse Dis3l1 siRNA#1	J-054584-10	Dharmacon	AGGAACUACUGGACGGAAA
mouse Dis3l1 siRNA#2	J-054584-11	Dharmacon	UGAAACAGAAGGCGUAUUU

Table 4

Primer sequences used in quantitative PCR

Target gene	Forward sequence	Reverse sequence
pre-let-7a-1	TGAGGTAGTAGGTTGTATAGTTTTAGGG	GGAAAGACAGTAGATTGTATAGTTATC
pri-let-7a-1	CTTTCAACATTCACCCTGGATGTTC	GAGACCCCATGAATGCAGACTTT
pre-let-7g	TGAGGTAGTAGTTTGTACAGTTTGAGG	GCAAGGCAGTGGCCTGTACAGTTATC
pri-let-7g	GTTCTCTTTTGCCTGATTCCAGG	CATTTGGTAGCTGGTGCACTG
U6	CTCGCTTCGGCAGCACA	AACGCTTCACGAATTTGCGT
ACTB	CAGAAGGAGATTACTGCTCTGGCT	TACTCCTGCTTGCTGATCCACATC
Dis3l1	AGTTGACAGACATAGCTCGCCACA	TGGTTGGCTAGGATCATGCACTCA